An experimental study of Couette instability of stratified fluids

By E. M. WITHJACK† AND C. F. CHEN

Mechanical, Industrial and Aerospace Engineering Department,
Rutgers University, New Brunswick, New Jersey 08903

The stability of Couette flow of stratified salt solutions is investigated in an apparatus with both the inner and outer cylinders rotating. The ratio of the radius of the inner cylinder to that of the outer cylinder is 0·2. The flow is visualized by means of shadowgraph and dye-trace methods. Compared with homogeneous fluids, the effect of the stabilizing density gradient is to increase the critical speed of the inner cylinder and to decrease the critical wavelength for a given angular speed of the outer cylinder. When the cylinders are rotating in the same direction, in the critical state, the instabilities appear along the inner cylinder in a spiral wave form which is itself not very stable. With counter-rotating cylinders, the instabilities appear as regularly spaced vortices which, for the most part, are neither symmetric Taylor vortices nor simple spirals. In addition, these vortices rotate as a whole at a speed generally smaller than that of the inner cylinder. From shadowgraph observations, stability curves are constructed for three density gradients. The critical wavelength and the rotational periods of the vortices are also determined.

1. Introduction

Since the pioneering work of Sir Geoffrey Taylor in 1923, the problem of the stability of homogeneous fluids in circular Couette flow has been under exhaustive experimental and theoretical study by many investigators. The results of these investigations have yielded not only a basic understanding of centrifugal instability in both the linear and nonlinear regimes, but also a host of mathematical techniques for such stability analysis.

Centrifugal instability in a density-stratified fluid may be of interest in geophysical flows. Droughton (1969) investigated the effect of vertical density stratification on the onset of centrifugal instability around a horizontal rotating cylinder. He found that the density gradient served to inhibit the onset of instabilities and that the toroidal vortices in the critical state became elliptical owing to the buoyancy forces. He also found that the flow in the far field exhibited different characteristics depending on whether the flow near the rotating cylinder was subcritical or supercritical.

In this paper we report the results of an experimental investigation of Couette instability of a stably stratified salt solution. The axis of rotation in this case is

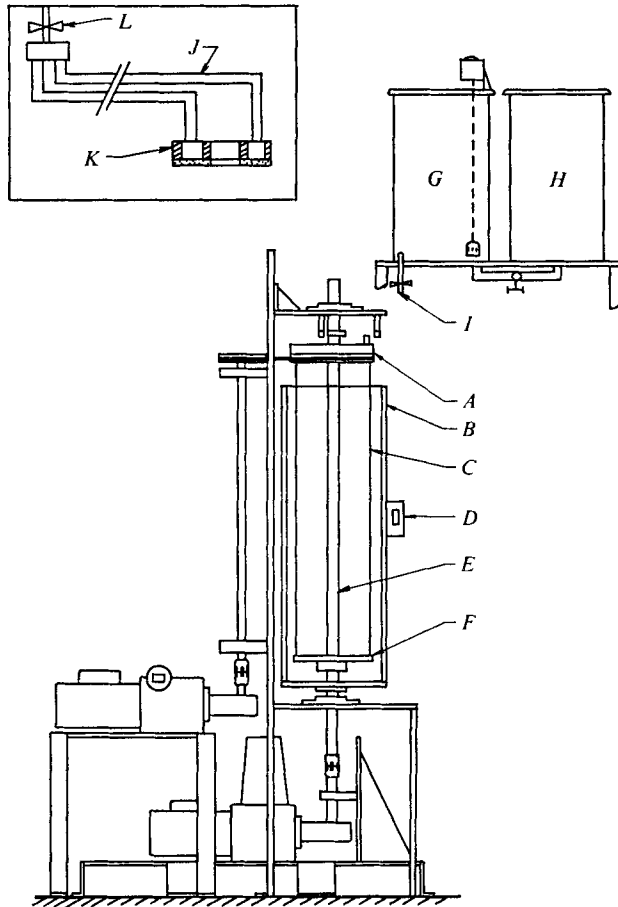† Present address: Transportation Systems Center, Cambridge, Mass.

FIGURE 1. Schematic diagram of experimental apparatus. A, upper end cap; B, Plexiglas fresh-water tank; C, 12·7 cm I.D. cylinder; D, clock; E, 2·54 cm O.D. brass shaft; F, lower end cap; G, salt-water tank; H, fresh-water tank; I, outlet tube; J, four capillary tubes; K, float; L, metering valve.

in the direction of the density gradient. The effect of buoyancy forces is found (i) to enhance the stability and (ii) to shorten considerably the critical wavelength from that found for homogeneous fluids. By shadowgraph techniques and dye-trace methods we have uncovered a rather complicated vortex pattern in the critical state.

2. Experimental apparatus and procedure

2.1. *Apparatus*

An experimental apparatus was designed and constructed which provided for (a) rotation of both the inner and the outer cylinders, (b) access to the annulus region to allow filling with a density-stratified fluid and (c) a means of flow visualization by the shadowgraph method. A schematic diagram of the test apparatus is shown in figure 1. The outer cylinder is a Plexiglas tube 61 cm

long with an inside diameter of 12.7 ± 0.15 cm, which is mounted concentrically with a brass tube having an outside diameter of 2.547 ± 0.0013 cm. The maximum run-out of the inner cylinder is $\pm 0.5\%$ in a bearing length of 80.0 cm.

The Plexiglas cylinder is closed at both ends by attaching with screws nylon end caps which are grooved to fit the ends of the cylinder. The upper nylon cap is made in two parts to allow filling with a density-stratified fluid: (i) a nylon ring which is permanently attached to the cylinder; (ii) a removable nylon disk which is machined to fit concentrically into the ring. The disk houses the upper cylinder ball bearing, which is sealed from the test fluid with a teflon Kapseal. The lower nylon cap and brass bearing enclosure house the lower cylinder thrust-type ball bearing, with sealing provided by Kapseals. Both of the cylinder bearings are of the prelubricated double-seal type.

An open Plexiglas tank 59 cm deep, 24 cm across and 29 cm wide surrounds the Plexiglas cylinder and is filled with fresh water to correct for differences in optical path length when using the shadowgraph for flow visualization. The tank is constructed of 1.91 cm thick Plexiglas sheet with all joints bonded and reinforced with screws. A shaft hole is provided at the bottom and leakage is prevented by using a teflon-faced wiper seal mounted in a brass plate. The relative alignment of the Plexiglas tank and brass inner cylinder was somewhat critical for proper functioning of the seal. One side of the Plexiglas tank is covered with a sheet of vellum to provide a translucent screen for shadowgraph viewing.

The cylinders are rotated by two separate Grahm variable-speed drives. The inner-cylinder drive unit is the same unit as was used by Chen, Liu & Skok (1973), and was described by them in detail. It is capable of speeds from 0 to 100 r.p.m. and is controlled through a Jordon electric speed control. However, in the course of these experiments it was found that the controller made speed adjustments in increments of approximately $\frac{1}{2}$ r.p.m. This may account for the jerkiness in the increase in angular speed reported by Chen *et al.* when they attempted to obtain constant variation of the angular speed of the inner cylinder with time. The outer-cylinder Grahm drive unit is capable of speeds from 0 to 200 r.p.m. and is controlled through a mechanical digital vernier speed dial. To rotate the outer cylinder, the Grahm drive transmission is coupled to a shaft-and-pulley arrangement. The inner cylinder is rotated by direct coupling of the transmission output shaft to the brass tube. Both Grahm drive units are mounted on individual heavy iron stands and anchored to the concrete floor. By anchoring the main cylinder support frame to the floor, and using rubber-splined couplings on the drive shafts, motor vibrations are not transmitted to the test fluid.

A Brush strip-chart dual-channel recorder is used to determine the angular speeds of the cylinders. One channel of the recorder is activated with a micro-switch to indicate cylinder revolutions per centimetre of chart paper; the other channel is triggered with a known frequency source to indicate the paper feed rate. With this arrangement cylinder speeds could be obtained to within approximately 0.1% in the range of angular speeds from 0 to 50 r.p.m. Stable speeds of rotation were consistently measured for angular speeds greater than $\frac{1}{2}$ r.p.m., but below that speed the rotation periods varied by $\pm 2\%$ owing to drifting within the transmission drive units.

The two-tank method is used to fill the annulus with a linearly stratified salt–water solution. This method was developed by Fortuin (1960), and also described by Oster (1965), as a relatively simple way of producing density gradient columns of fluid. Two 10 l plastic tanks are mounted on top of a 2 m high tower to allow gravity feeding. As shown in the inset in figure 1, flow out of the brine tank is controlled through a metering valve and directed into four capillary tubes attached to a polystyrene float having a thin sponge bottom. The small-pore sponge is approximately 0·3 cm thick and spreads fluid evenly through the bottom of the float. The dimensions of the float are not critical, but are such that it may be lowered into the annulus when the upper end cap and bearing mount are removed in preparation for the filling process.

The bulk of the experimental data was obtained using the shadowgraph method. The 500 W light source is positioned about 2 m from the centre of the apparatus at the mid-height of the test region. Although the shadowgraph reveals the growth of instabilities, it does not show the physical nature of the associated wave form. Conventional methods of flow visualization such as dye injection and mixing aluminium powder or pearl essence into the test fluid, were prohibited owing to the linear density stratification. A method of flow visualization was developed after it was noticed that methynol blue dye diffused well into pearl essence. The method is, basically, to prepare about 2 ml of the ingredients mentioned, and paint them onto the surface of the brass inner cylinder while the stratified fluid is filling the annulus. It is important to apply the mixture to the cylinder just above the rising water level to minimize exposure to air, which dries the mixture, and results in flaking when the cylinder is started to rotate. The shadowgraph and dye traces are photographed using a 35 mm camera or a 16 mm movie camera.

2.2. *Procedure*

A linearly stratified salt solution was prepared in the annulus using the two-tank method. The flow was adjusted so that no excessive mixing occurred. Samples of solution were taken at the beginning and the end of filling, which usually took about one hour. Specific-gravity measurements were made of the samples with a Sartorius analytical balance. From the difference between the specific gravities at the top and bottom of the stratified fluid, an initial non-dimensional stratification ϕ_0 was determined using the radius R_1 of the inner cylinder as the basic length:

$$\phi_0 = \frac{R_1}{\rho_0} \frac{d\rho}{dz},$$

where ρ_0 is the density of the fluid at the mid-height of the stratified column.

The linearity of the density gradient was checked by extracting four samples of fluid from depths of 0·64, 20·03, 40·06 and 57·75 cm and measuring their indices of refraction. A four-tube sample extractor of hypodermic tubing was lowered into the test fluid using a vertical traversing mechanism which was temporarily attached to the frame of the apparatus above the opening into the annulus. After a wait of 16–18 h after filling for any density irregularities to diffuse, samples of about 0·2 ml were drawn through the tubes into four syringes.

The extractor was then cautiously removed, and the upper end cap and bearing mount installed. Measurements were taken of the refractive indices of the removed samples using a Bausch & Lomb Abbe refractometer. From these measurements the linearity of the density gradient was verified. During the course of this investigation, three sequences of tests were conducted, each sequence having a different initial average density gradient $\bar{\phi}_0$. The maximum variation of ϕ_0 within a sequence from the initial average density gradient was found to be $\pm 1.44 \%$.

After the above preparations, a test run was commenced by measuring the water temperatures at the top and bottom of the fresh-water tank. A positive temperature difference of $0.3 \,°C$ was usually recorded over the 59 cm height. Next the room was darkened and the light source switched on. The angular speed of the outer cylinder was increased from zero to the desired test speed. The speed of the inner cylinder was brought up from zero at a constant rate of $\frac{1}{2}$ r.p.m. every 2 min until a speed 80 % of the expected critical speed was attained. The rate of speed increase was then decreased to $\frac{1}{2}$ r.p.m. every 5 min. This decrease was necessary in view of the results of the pilot experiments, which showed that the onset of instability may require 2–3 min to develop, and that instability may set in prematurely owing to a transient velocity field. For a more detailed description of the apparatus and test procedure, see Withjack (1974).

3. Results and discussion

3.1. *Experimental observations*

The instabilities occurring in a stratified flow between rotating concentric cylinders have different general features depending on the relative sense of rotation of the cylinders. With counter-rotating cylinders, the secondary flow is very orderly and persistent. With unidirectional rotation of the cylinders, the secondary flow is more chaotic. Three sequences of experiments were carried out, at $\phi_0 = -0.0010$, -0.0020 and -0.0029 (with corresponding buoyancy oscillation periods of 7.2, 5.0 and 4.2 s respectively), with cylinders having a radius ratio $\eta = R_1/R_2 = 0.2$. R_1 and R_2 are the radii of the inner and outer cylinders. Reynolds numbers are defined for the inner and outer cylinders respectively as follows:

$$Re_1 = R_1^2 \Omega_1 / \nu_0, \quad Re_2 = R_2^2 \Omega_2 / \nu_0,$$

where ν_0 is the kinematic viscosity of the fluid at the mid-height and Ω_1 and Ω_2 are the angular velocities of the inner and outer cylinders.

The kinematic visosity of salt solution increases with salt concentration (Kaufmann 1960, p. 622). With our stratified column, when both cylinders are rotating at constant speed there is nearly a linear decrease in Reynolds number with depth. This fact allows the stratified Couette flow to reach a critical Reynolds number first in the less-dense fluid near the top of the annulus, while a sub-critical Reynolds number flow is present in the heavier fluid near the bottom. In this situation, a secondary flow evolves in the form of azimuthal vortices evenly spaced along the top section of the inner cylinder, while near the bottom

the basic flow field is laminar with only a tangential velocity. By increasing the angular speed of the inner cylinder in a step-like manner, the instability develops in regions of successively heavier fluid until the entire flow field is unstable. This phenomenon is most prominent with the largest density gradient used.

The segmented onset of instabilities is illustrated by a series of photographs shown in figure 2 (plate 1) for $\bar{\phi}_0 = -0.0029$, $Re_1 = 231.6$ and $Re_2 = -6863.4$. The critical Reynolds number of the inner cylinder is evaluated at the angular speed at which the flow at the mid-height becomes unstable. The general sequence of events which occurs in all the experiments with counter-rotating cylinders is depicted by this case. The initial laminar motion of the basic flow is shown in figure 2(a). The curved horizontal lines at the bottom of the shadowgraph are end effects and will be discussed in a later paragraph. At the onset of instability, the first 15 cm down the inner cylinder to the first marker in figure 2(b) shows simultaneous radial motion of the fluid at equally spaced locations. The irregular horizontal bright strip at the top of the shadowgraph is a reflexion of stray light from the source off the air–water interface of the fresh water in the tank surrounding the rotating cylinders. After waiting 26 min, no further spontaneous onset of instability was observed, and the speed of the inner cylinder was increased by $\frac{1}{2}$ r.p.m. In figure 2(c) the second marker indicates the extent of the spontaneous increase in the depth of the instability, and its subsequent development ending approximately half-way down the cylinder is shown by the third arrow in figure 2(d). The speed of the inner cylinder was increased by $\frac{1}{2}$ r.p.m. after waiting 11 min, which resulted in the spontaneous onset of instability between the third and fourth markers. This was followed by a slow increase in the depth of the instability which stopped within a few centimetres from the bottom of the annulus after 24 min. The speed of the inner cylinder was then increased by $\frac{1}{2}$ r.p.m., which resulted in the final development of the instability over the entire cylinder as shown in figure 2(e). The flow after 2 h 18 min is shown to remain very orderly and persistent in figure 2(f).

The horizontal lines on the shadowgraph indicate relatively large local density gradients in the overall stably stratified flow. The overall density distribution is locally distorted by the secondary flow. Strong density gradients occur across circular planes between adjacent vortices of the instability; these planes are projected as horizontal lines onto the plane of the shadowgraph. Radial motion of the fluid is observed along any one of the horizontal lines as radial inflow on one side of the inner cylinder and radial outflow on the other. Lines of radial inflow are observed to have lines of radial outflow above and below on the shadowgraph, and conversely lines of radial outflow on one side of the cylinder have lines of radial inflow above and below. The lines of outflow curl at the tips in a dovetail manner, and increase in length from a minimum of about $\frac{1}{2}$ cm to a maximum of about 3 cm, at which time the directions of flow along the lines reverse.

The end effects appearing in figure 2(a) at the bottom of the cylinders are also present at the top, but not visible in any of the photographs. The curved horizontal lines indicate sharp vertical density gradients, and suggest a similarity between these end effects and the viscous overturning instability reported by

Baker (1971). The fluid in contact with an end cap is in solid-body rotation, while fluid at some distance away is governed by the surface speeds of the inner and outer cylinder walls. This vertical velocity gradient causes a viscous overturning which is observed on the shadowgraph as curved horizontal sheets. End effects are manifested with different curvatures of the horizontal sheets depending on both the relative sense of the angular velocities and their magnitudes.

The wave form of the instability shown in figure 2 is the most prevalent for counter-rotating cylinders. In figure 3 (plate 2) another wave form is shown co-existing with the most prevalent for a test with a smaller density gradient of -0.0020, $Re_1 = 235.1$ and $Re_2 = -7884.2$. In figure 3(a) the most prevalent asymmetric form of the instability is shown along the inner cylinder from the top down to the second marker, and developed immediately after the first increase in the angular speed of the cylinder. The pairs of horizontal lines of equal contrast on either side of the inner cylinder below the second marker indicate a symmetric Taylor wave form. This was confirmed by dye traces in other experiments during the test series. Within 2 min, the instability becomes of the asymmetric type shown in figure 3(b). Tests conducted with a density gradient of -0.0010 exhibited the symmetric wave form at the onset of instability more frequently than tests with the larger density gradients described above. However, the symmetric wave form was usually, but not invariably, transformed into the asymmetric form. The results indicate that the flow is initially unstable with respect to axisymmetric disturbances. These in turn become unstable with respect to azimuthal disturbances, whose growth rate is a function of the initial density gradient. Snyder (1968a) reported wave-form transitions in homogeneous Couette flow instabilities for counter-rotating cylinders over a range of radius ratios 0.2–0.959.

Typical vortex systems made visible by the dye trace are shown in figure 4 (plate 3). Dye was painted along the top section of the inner cylinder, and hence the vortices appear to fade near the bottom of the photograph. The vortex system is shown fully developed 47 min into a test at $Re_1 = 144.9$, $Re_2 = 2195.1$ and $\bar{\phi}_0 = -0.0010$. We remark here that this wave form is actually asymmetric. It appears symmetric only at this position and 180° away from it. However, superposition of the wave form made visible by the dye onto the shadowgraph reveals the true asymmetric nature of the instability. The sketch in figure 5 shows the dye-traced wave form and shadowgraph superimposed. The arrows show the direction of the motion on the shadowgraph, and reveal that although there appears to be a symmetric system of toroidal vortices in figure 4 this is not actually the case.

When the wave form as shown in figures 4 and 5 is rotated through 90°, it presents an entirely different picture as sketched in figure 6. The dye traces show an interconnecting tubular pattern which crosses around the inner cylinder as illustrated in figure 6(a). The pattern shows a pair of rather large vortex cells on one side of the cylinder which gradually diminish into two small vortex cells on the other side of the cylinder. The corresponding circulation patterns are shown in figure 6(b). The flow pattern from this viewpoint is also time-dependent. As time progresses, the small side of a vortex puffs up apparently at the expense
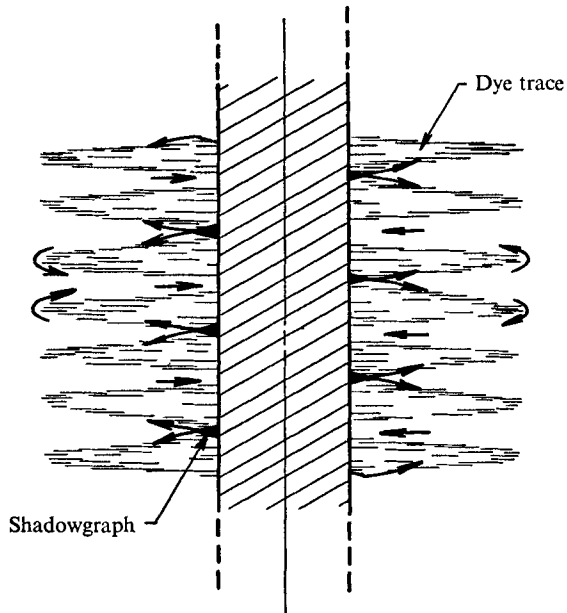
FIGURE 5. Sketch of dye-traced wave form superposed on a shadowgraph showing asymmetry.
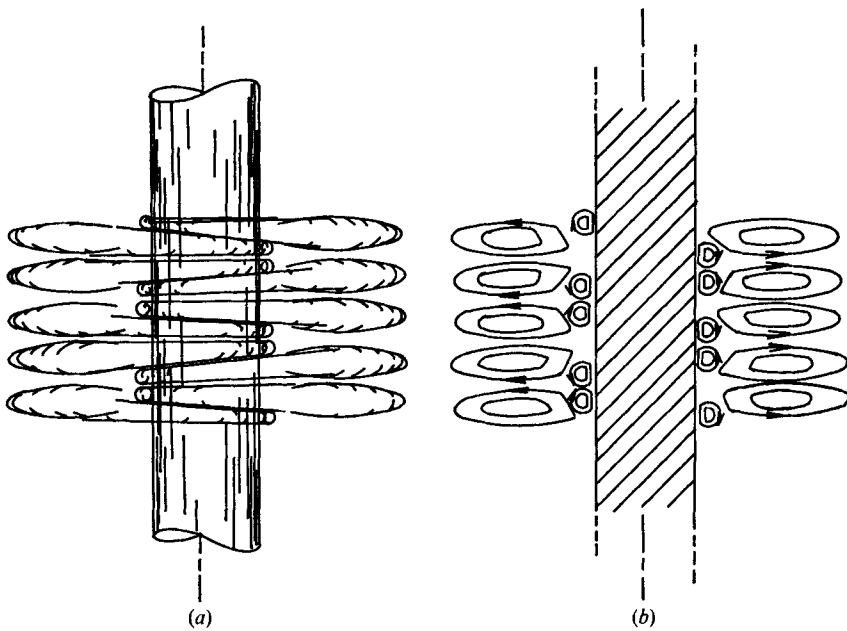

(a)   *(b)*

FIGURE 6. Sketches of (a) interconnecting vortices and (b) cell patterns.

of the adjacent larger vortices until the smaller ones become the larger ones and vice versa.

An additional oscillatory mode *sometimes* occurs after the flow has become unstable over the entire length of the inner cylinder. It appears to 'whip' the secondary flow pattern from one side of the cylinder to the other. This is illustrated in a series of photographs shown in figure 7 (plate 4). The photographs were taken during the test described in figure 2 at approximately the mid-height of the test region. Figure 7 (*a*) shows that, at the beginning of an oscillation, the instability elongated or stretched towards the marker. Approximately 6 s later, as figure 7 (*b*) shows, the instability elongated away from the marker, and the cycle is complete in figure 7 (*c*). It is not discernable whether this oscillation actually has an azimuthal velocity, or if it is pulsating but stationary. Seemingly, there is no correlation between this oscillatory mode and the periodic reversal of the lines of inflow and outflow in the instability.

For cases of unidirectional rotation of the cylinders, the instability was observed to be asymmetric. Experiments carried out for $\bar{\phi}_0 = -0.0010$ and -0.0020 show a large vertical spacing, approximately 5 cm between the horizontal lines on the shadowgraph. Using the dye-trace method previously described, the instability was observed to be a large spiral wave form extending radially nearly to the outer cylinder. The motion on the shadowgraph is difficult to follow by eye because of the rapid shifting of the wave form. A strong churning motion was observed which resulted in rapid loss of contrast in the shadowgraph and discouraged presentation of the photographs.

3.2. *Quantitative results and discussion*

A total of 20 tests was conducted to include three average density gradients of -0.0010, -0.0020 and -0.0029. The data presented in table 1 are grouped into three major sections according to the average density gradient. Within each section the test results are arranged with decreasing values of the speed ratio μ ($= \Omega_2/\Omega_1$).

Stability curves for each average density gradient are shown in figure 8, together with the stability curve for a homogeneous fluid from the calculated results of Sparrow, Munro & Jonsson (1964) and Snyder (1968*b*). The three curves show that increasing density stratification tends to enhance the stability of the flow. As the density gradient increases, the limiting Reynolds number of the inner cylinder below which the flow remains stable increases at any particular Reynolds number of the outer cylinder. In comparison with the homogeneous case, the stabilizing effect of density stratification increases the critical Reynolds number of the inner cylinder by as much as six times for the smallest density gradient under consideration. With both cylinders rotating in the same direction, the experimental stability curve crosses the Rayleigh criterion $R_1^2 \Omega_1 = R_2^2 \Omega^2$ for a homogeneous inviscid fluid. When the Reynolds numbers of both the inner and outer cylinder become large (~ 800), the centrifugal effect becomes dominant. As a result, the experimental point satisfies the Rayleigh criterion almost exactly. Additional experiments are needed to determine the stability boundary at high Reynolds numbers for co-rotating cylinders.

Run	Speed ratio	Reynolds number of outer cylinder	Reynolds number of inner cylinder	Speed of outer cylinder (r.p.m.)	Speed of inner cylinder (r.p.m.)	Mid-height kinematic viscosity (cm² s⁻¹)	Density gradient
1	0·079	339·1	201·9	0·94	11·81	0·00990	−0·00102
2	0·042	831·9	784·9	1·95	45·75	0·00990	−0·00101
3	0·0	0	124·3	0	7·28	0·00991	−0·00100
4	−0·606	−2195·1	144·9	−5·15	8·50	0·00991	−0·00100
5	−1·176	−5577·5	189·9	−13·08	11·12	0·00990	−0·00100
6	−1·450	−8536·6	235·5	−20·01	13·80	0·00990	−0·00101
7	0·073	753·2	413·8	1·80	24·67	0·01008	−0·00201
8	0·073	379·0	206·8	0·91	12·40	0·01012	−0·00201
9	0·023	82·2–84·5	146·8	0·19–0·20	8·73	0·01008	−0·00200
10	0	0	147·3	0	8·82	0·01013	−0·00199
11	0	0	149·8	0	8·98	0·01008	−0·00199
12	−0·091	−339·9	149·1	−0·82	9·02	0·01020	−0·00201
13	−0·487	−2046·4	168·2	−4·94	10·13	0·01016	−0·00197
14	−0·963	−4771·5	198·3	−11·55	12·00	0·01021	−0·00200
15	−1·232	−6255·1	202·9	−15·10	12·22	0·01016	−0·00195
16	−1·342	−7884·2	235·1	−19·05	14·18	0·01018	−0·00197
17	−1·570	−10139·8	258·3	−24·50	15·60	0·01018	−0·00198
18	−0·422	−1867·1	177·1	−5·15	12·20	0·01166	−0·00290
19	−0·938	−4838·5	206·3	−13·32	14·16	0·01163	−0·00289
20	−1·186	−6863·4	231·6	−19·00	16·03	0·01168	−0·00295

Run	Variation in specific gravity†	Mid-height specific gravity	Variation in percentage weight of salt†	Mid-height percentage weight of salt	λ/R_1	Waveform oscillation period (s)
1	0·048938	1·041553	6·75	5·98	2·91	30·0
2	0·048239	1·041544	6·63	5·98	—	—
3	0·047680	1·042388	6·54	6·12	1·97	55·0
4	0·048112	1·043030	6·61	6·20	1·02	—
5	0·047648	1·041833	6·54	6·05	0·91	18·0
6	0·048483	1·042129	6·57	6·05	1·02	14·0
7	0·098052	1·059968	13·25	8·43	3·94–5·51	15·0
8	0·098632	1·064487	13·34	9·03	2·12	27·0
9	0·097587	1·060043	13·20	8·43	1·81	—
10	0·097303	1·064723	13·00	9·11	1·73	43·0
11	0·097030	1·059565	13·12	8·36	1·73	43·0
12	0·099065	1·068221	13·33	9·54	1·49	52·0
13	0·096711	1·066859	13·01	9·36	1·02	25·0
14	0·098178	1·068697	13·22	9·59	0·91	15·5
15	0·095086	1·067493	12·85	9·42	0·87	16·0
16	0·096618	1·067624	13·01	9·46	0·87	15·0
17	0·097215	1·067995	13·12	9·52	0·79	12·0
18	1·126392	1·126392	19·01	16·89	1·10	22·0
19	1·124220	1·124220	19·04	16·68	0·87	14·0
20	1·127220	1·127220	19·20	16·95	0·87	14·0

† Variation is difference between values of mentioned quantity at top and bottom of test annulus (61 cm).
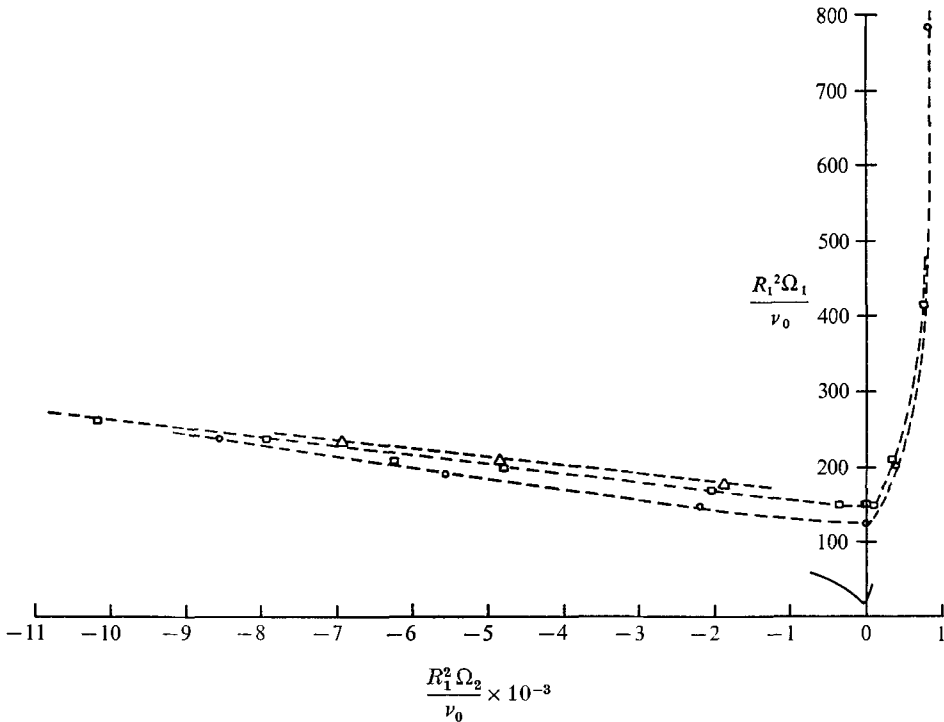
TABLE 1. Experimental results

FIGURE 8. Experimental neutral-stability curves. $\bigcirc$, $\bar{\phi}_0 = -0.001$;
$\square$, $\bar{\phi}_0 = -0.002$; $\triangle$, $\bar{\phi}_0 = -0.0029$; ———, homogeneous fluid.

The experimental data shown for Reynolds numbers of the outer cylinder near zero are to be considered with some caution owing to the previously mentioned drift of 2 % in the transmission speed controller. For cylinders rotating in the same direction, there is a possible influence of end effects on the instability in view of the large ratio of the unstable wavelength to the length of the test region.

The approximate wavelengths λ observed between vortex pairs are plotted in figure 9, together with the theoretical results for the homogeneous case from Sparrow *et al.* (1964). At positive speed ratios the axial wavelength is taken as the distance between adjacent vortices in the spiral. Owing to the shifting of the spiral vortex in an erratic flow field, a vertical bar is shown on one data point to indicate observed wavelength variations. The effect of increased density gradients is to decrease the critical wavelength. At positive speed ratios the difference in spacing is more apparent, but as the speed ratio becomes smaller the wavelength for the three density gradients approaches $\lambda/R_1 = 0.9$. This asymptotic trend is probably due to the increase in centrifugal effects at large angular speeds of the outer cylinder. It is interesting to note that the critical wavelength for the stratified case is approximately a quarter of that in the homogeneous case. In a stably stratified fluid a restoring force acts on a fluid element displaced vertically from its equilibrium position, thus limiting its vertical movement. Such restriction of vertical (axial) motion is influential in reducing the spacing of the vortices in the instability, and resulting in elongated elliptical vortices.
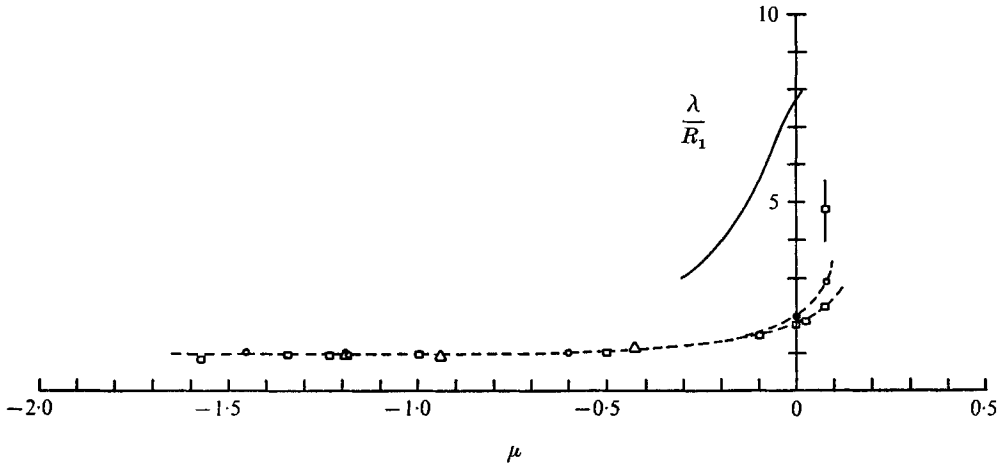
FIGURE 9. Critical wavelengths $\bigcirc$, $\bar{\phi}_0 = -0\cdot001$; $\square$, $\bar{\phi}_0 = -0\cdot002$;
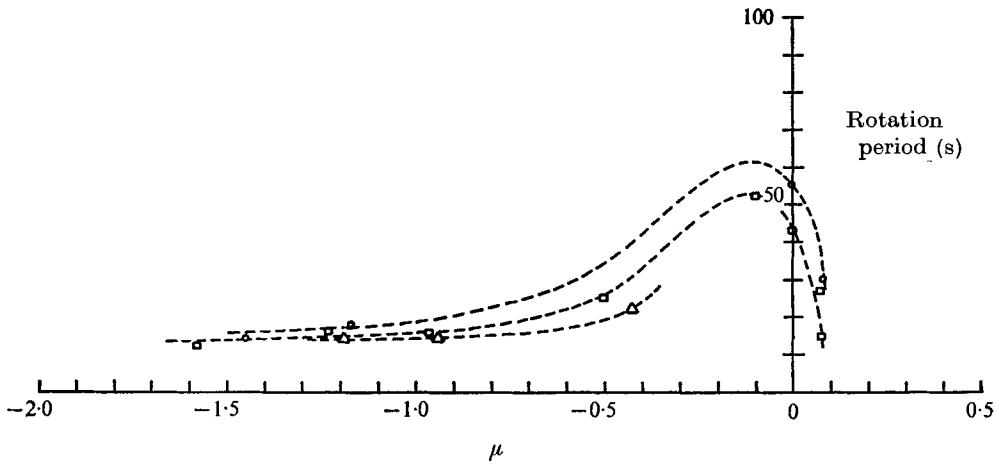$\triangle$, $\bar{\phi}_0 = -0\cdot0029$; ——, homogeneous fluid.

FIGURE 10. Period of rotation of the secondary flow pattern.
$\bigcirc$, $\bar{\phi}_0 = -0\cdot001$; $\square$, $\bar{\phi}_0 = -0\cdot002$; $\triangle$, $\bar{\phi}_0 = -0\cdot0029$.

Approximate periods of wave-form rotation are shown by the three curves in figure 10. The family of curves shows that the periods are minimum for positive μ, increase to a maximum at small negative values of μ and tend to level off at 14 s as μ decreases. Increased density gradients result in decreased periods, but become less influential as μ decreases. The data indicate that for $\mu < -1$ the periods tend to approach $0\cdot3\Omega_1$; this is interesting in view of results for the homogeneous case reported by Snyder (1968a) indicating that the disturbance wave form had a period near $\frac{1}{3}\Omega_1$ over a range of speed ratios from $0\cdot040$ to $-1\cdot5$. Owing to the influence of strong centrifugal forces at the larger negative speed ratios, preferred periods of wave-form rotation which are approximately the same may result for both the stratified and homogeneous cases.

4. Conclusions

We have performed experiments to examine the effect of density stratification on the instability of Couette flow between rotating cylinders whose radius ratio η is 0·2. Three linear density gradients of $-0·0010$, $-0·0020$ and $-0·0029$ were considered. Experiments were conducted with both the inner and outer cylinders in rotation for Reynolds numbers of the inner and outer cylinders in the ranges 784·9 to 124·3 and 831·9 to $-10139·8$, respectively. In the course of the investigation a successful dye-trace method for visualization of stratified flow was developed.

Test results indicate that, as the density gradient is increased, the onset of instability is inhibited. This is shown by the increase in the limitating Reynolds number of the inner cylinder below which the flow remains stable. At the onset of instability, an asymmetric wave form appears to be the most prominent for counter-rotating cylinders, and a spiral wave form develops for cylinders rotating in the same direction. The wave form rotates about the inner cylinder with a speed different from the speeds of rotation of both cylinders. A decrease in wavelength is observed with an increase in density gradient. The smaller wavelengths may be attributed to restoring forces in a stably stratified fluid which act on a vertically displaced fluid particle to return it to its neutrally buoyant position.

REFERENCES

BAKER, D. J. 1971 Density gradients in a rotating stratified fluid: experimental evidence of a new instability. *Science*, **172**, 1029.

CHEN, C. F., LIU, D. C. S. & SKOK, M. W. 1972 Stability of circular Couette flow with constant finite acceleration. *J. Appl. Mech.* **40**, 347.

DROUGHTON, J. V. 1969 Studies in stratified flow. Ph.D. thesis, Mechanical and Aerospace Engineering Department, Rutgers University, New Brunswick, New Jersey.

FORTUIN, J. M. H. 1960 Theory and application of two supplementary methods of constructing density gradient columns. *J. Polymer Sci.* **44**, 505.

KAUFMANN, D. W. 1960 *Sodium Chloride*. New York: Reinhold.

OSTER, G. 1965 Density gradients. *Sci. Am.* **213**, 70.

SNYDER, H. A. 1968*a* Stability of rotating Couette flow. I. Asymmetric waveforms. *Phys. Fluids*, **11**, 728.

SNYDER, H. A. 1968*b* Stability of rotating Couette flow. II. Comparison with numerical results. *Phys. Fluids*, **11**, 1599.

SPARROW, E. M., MONRO, W. D. & JONSSON, V. K. 1964 Instability of the flow between rotating cylinders: the wide gap problem. *J. Fluid Mech.* **20**, 35.

WITHJACK, E. M. 1974 Couette instability in stratified fluids. Ph.D. thesis, Department of Mechanical, Industrial & Aerospace Engineering, Rutgers University, New Brunswick, New Jersey.
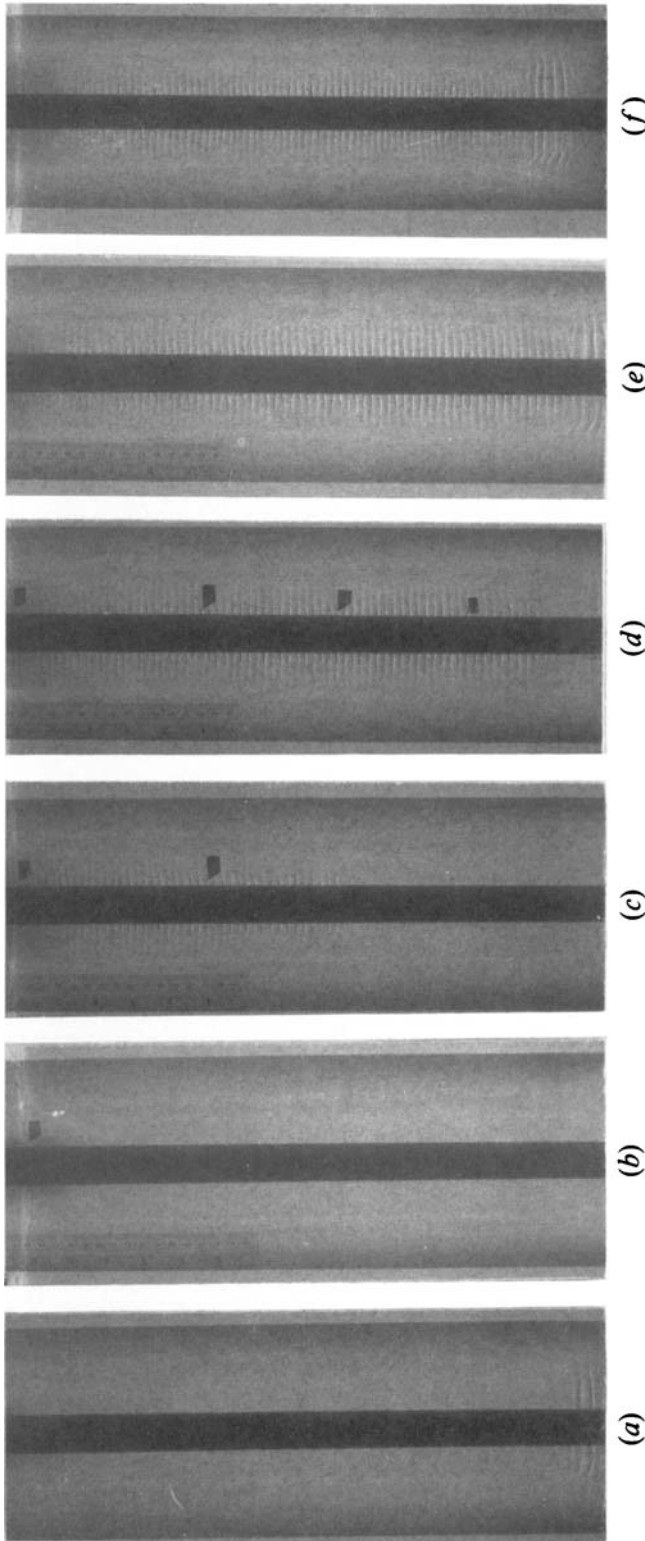
FIGURE 2. Experiment at $Re_1 = 231 \cdot 6$, $Re_2 = -6863 \cdot 4$ and $\bar{\phi}_0 = -0 \cdot 0029$. (*a*) Laminar flow with end effect at bottom (10:47). (*b*) Onset of instability (11:06). (*c*) Flow after first $\frac{1}{2}$ r.p.m. speed increase (11:35). (*d*) Flow after second $\frac{1}{2}$ r.p.m. speed increase (12:04). (*e*) Flow after third $\frac{1}{2}$ r.p.m. speed increase (12:17). (*f*) Flow persists (13:55).
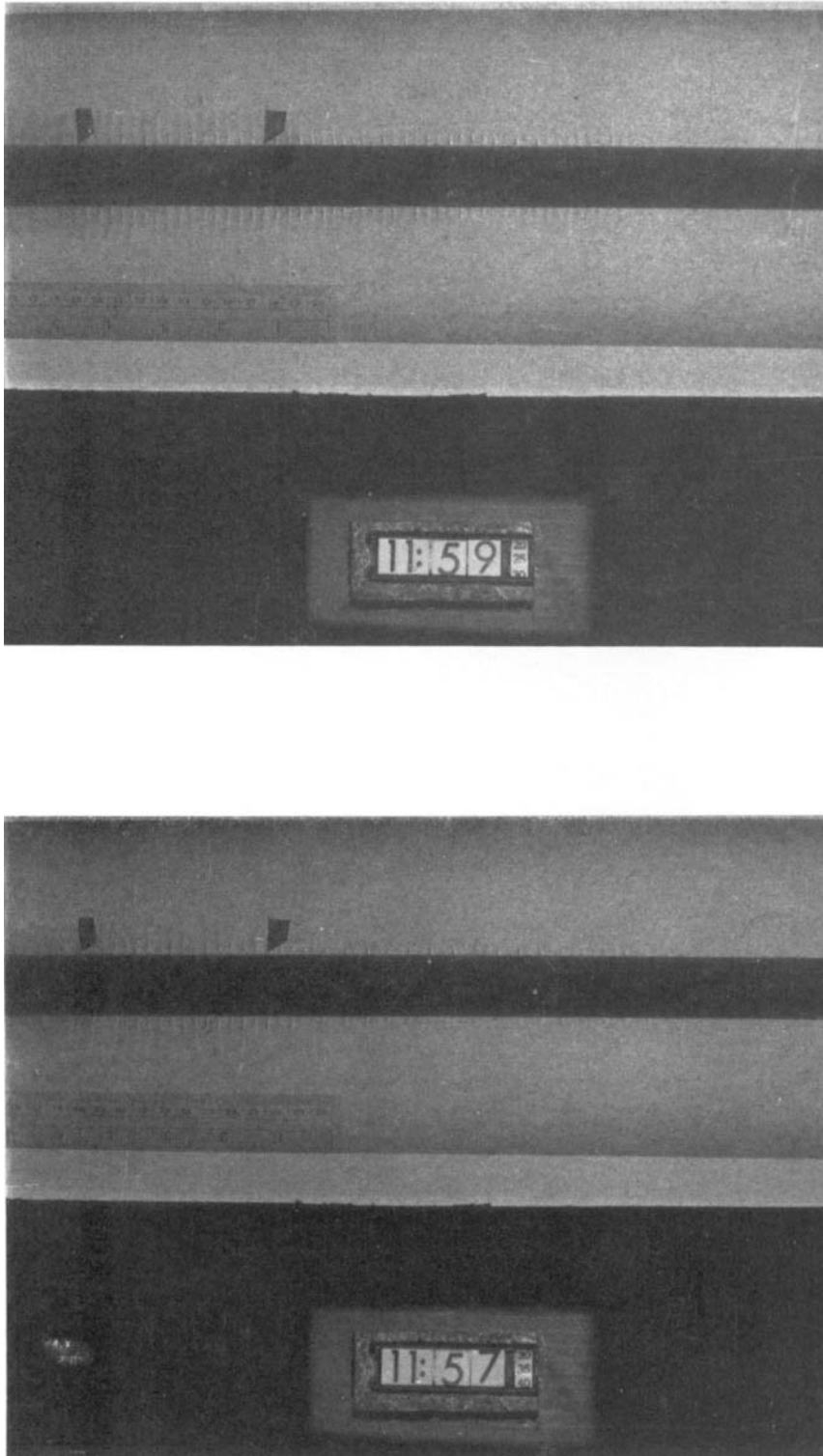
FIGURE 3. Experiment at $Re_1 = 235 \cdot 1$, $Re_2 = -7884 \cdot 2$ and $\bar{\phi}_0 = -0 \cdot 0020$. (a) Asymmetric and symmetric disturbance simultaneously present. (b) Symmetric wave form transforms to asymmetric wave form.
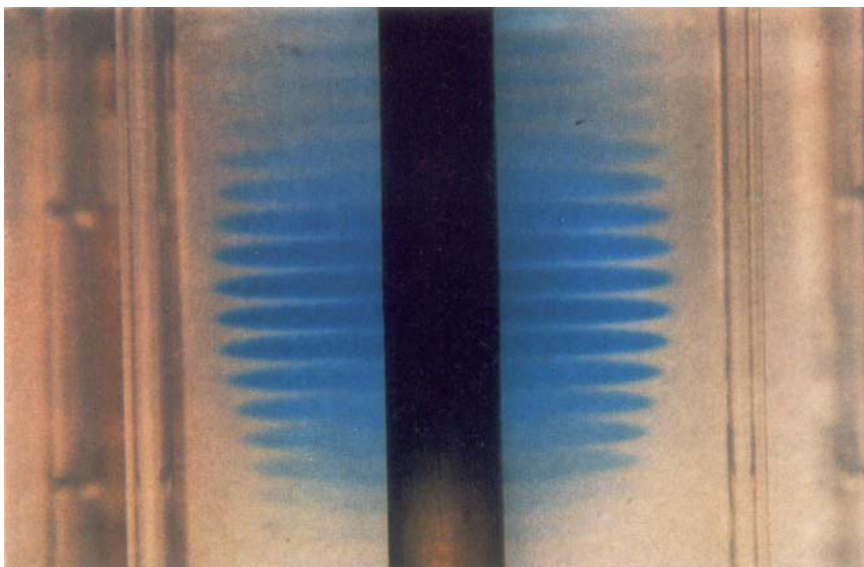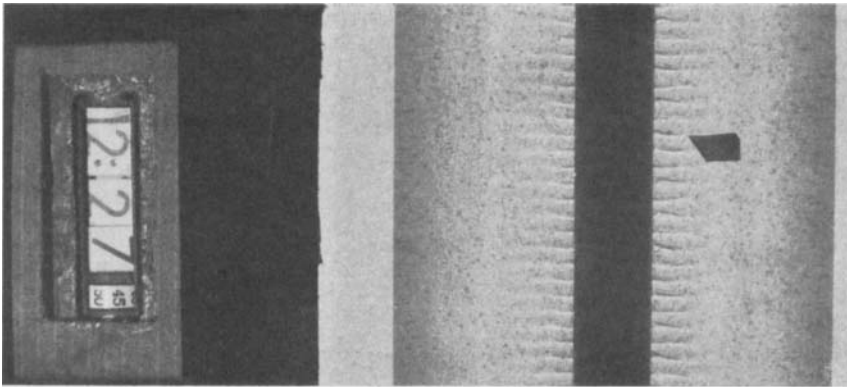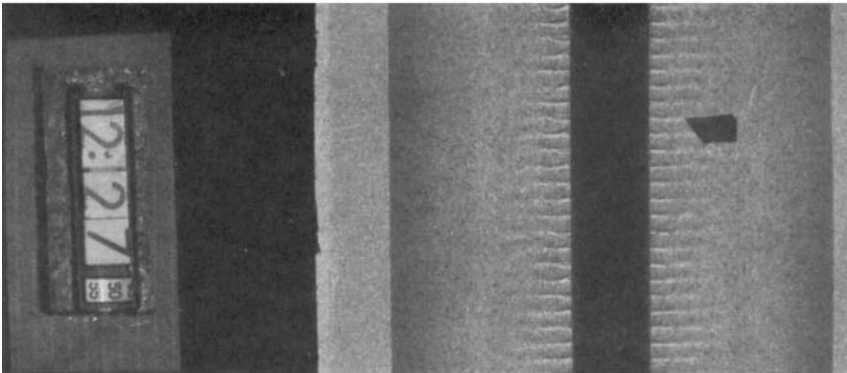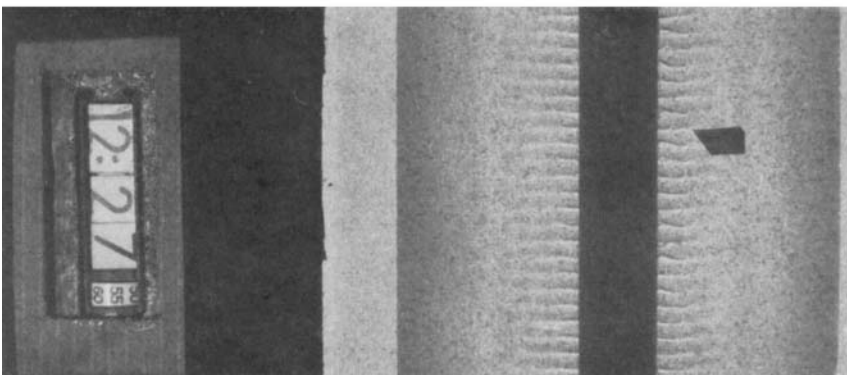
FIGURE 4. Dye trace of the secondary flow pattern with counter-rotating cylinders. $Re_1 = 144 \cdot 9$, $Re_2 = -2195 \cdot 1$, $\overline{\phi}_0 = -0 \cdot 001$.

(a)

(b)

(c)

FIGURE 7. Oscillatory mode shifts the secondary flow pattern from (a) right, to (b) left, and (c) returns it to the original position at beginning of cycle.

WITHJACK AND CHEN